AD-A053 451 BOSTON UNIV MASS DEPT OF ASTRONOMY F/G 4/1
NUMERICAL SIMULATION OF IONOSPHERIC AND PLASMASPHERIC DYNAMICS.(U)
JAN 78 M MENDILLO, C C CHACKO, B VANCE F19628-77-C-0019
UNCLASSIFIED AFGL-TR-78-0026 NL

1 OF 1
AD A053451

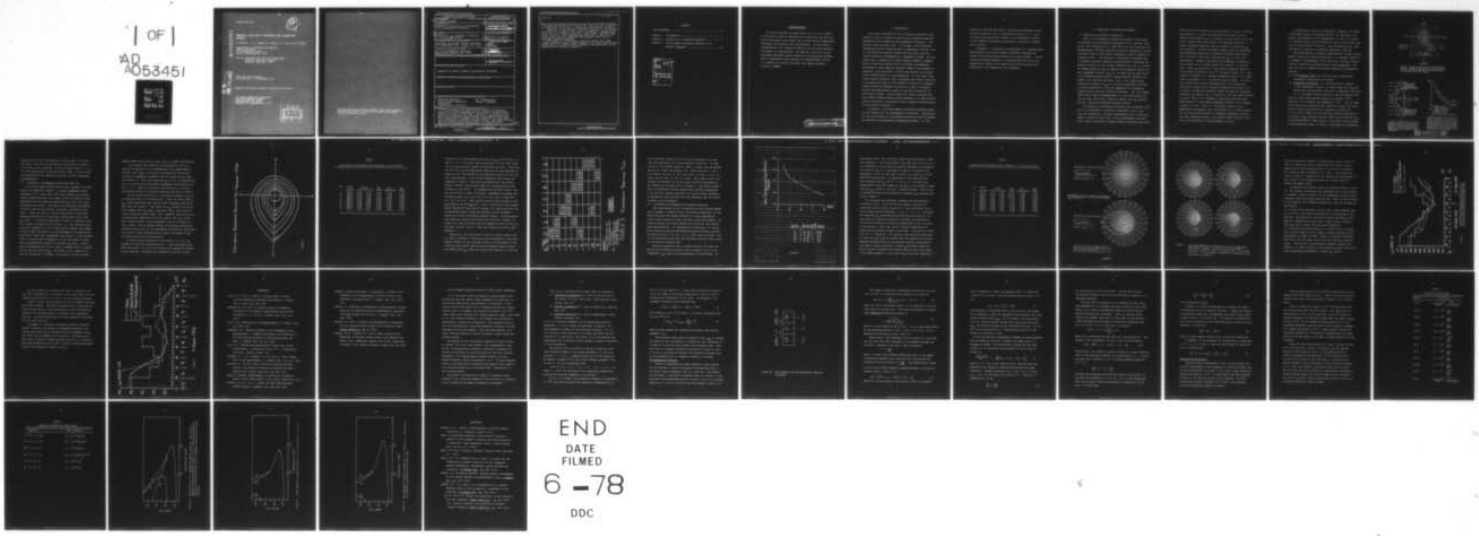

END
DATE FILMED
6 -78
DDC

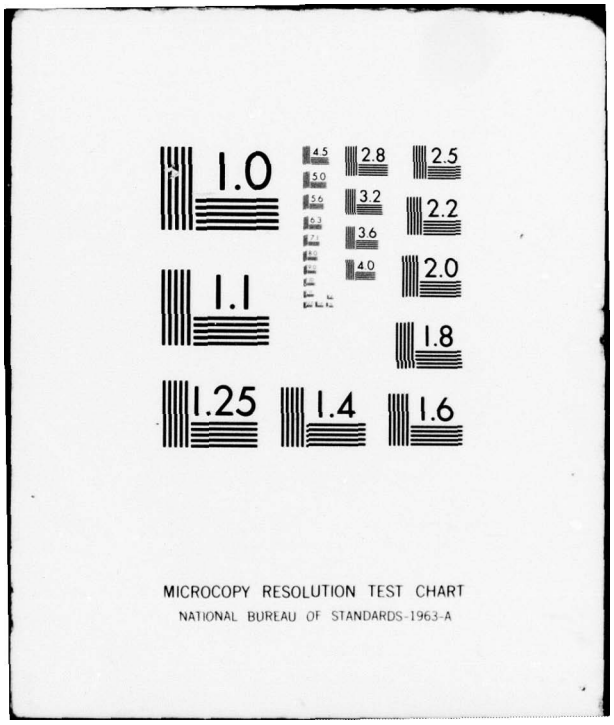
1.0
1.1
1.25
1.4
1.6
1.8
2.0
2.2
2.5
2.8
3.2
3.6
4.0
4.5
5.0
5.6
6.3
MICROCOPY RESOLUTION TEST CHART
NATIONAL BUREAU OF STANDARDS-1963-A

AFGL-TR-78-0026

AD A053451

NUMERICAL SIMULATION OF IONOSPHERIC AND PLASMASPHERIC DYNAMICS

M. Mendillo, C. C. Chacko, B. Vance, F. X. Lynch and B. Balko*

Departments of Astronomy and Physics
Boston University
725 Commonwealth Avenue
Boston, Massachusetts 02215

*Now at Laboratory for Technical Development
National Institute of Health
Bethesda, Maryland 20014

Final Scientific Report
1 October 1976 - 30 September 1977

Approved for public release; distribution unlimited

AIR FORCE GEOPHYSICS LABORATORY
AIR FORCE SYSTEMS COMMAND
UNITED STATES AIR FORCE
HANSCOM AFB, MASSACHUSETTS 01731

Unclassified

SECURITY CLASSIFICATION OF THIS PAGE (When Data Entered)

REPORT DOCUMENTATION PAGE	READ INSTRUCTIONS BEFORE COMPLETING FORM
1. REPORT NUMBER: AFGL-TR-78-0026	2. GOVT ACCESSION NO.
3. RECIPIENT'S CATALOG NUMBER	
4. TITLE (and Subtitle): Numerical Simulation of Ionospheric and Plasmaspheric Dynamics.	5. TYPE OF REPORT & PERIOD COVERED: ~~Scientific Final~~ Final Scientific Rept. 10 Oct 76-30 Sep 77
	6. PERFORMING ORG. REPORT NUMBER: A. C. B. U., Ser. III No. 5
7. AUTHOR(s): M. Mendillo, C. C. Chacko, B. Vance, F. X. Lynch and B. Balko	8. CONTRACT OR GRANT NUMBER(s): F19628-77-C-0019
9. PERFORMING ORGANIZATION NAME AND ADDRESS: Astronomy Department, Boston University, 725 Commonwealth Ave., Boston, MA 02215	10. PROGRAM ELEMENT, PROJECT, TASK AREA & WORK UNIT NUMBERS: ~~35100F~~ DMSP00AD
11. CONTROLLING OFFICE NAME AND ADDRESS: Air Force Geophysics Laboratory, Hanscom AFB, Bedford, MA 01731, Contract Monitor: Dr. P. J. L. Wildman/PHR	12. REPORT DATE: Jan 1978
	13. NUMBER OF PAGES: 44 P.
14. MONITORING AGENCY NAME & ADDRESS (if different from Controlling Office)	15. SECURITY CLASS. (of this report): Unclassified
	15a. DECLASSIFICATION/DOWNGRADING SCHEDULE

16. DISTRIBUTION STATEMENT (of this Report)

Approved for public release; distribution unlimited

17. DISTRIBUTION STATEMENT (of the abstract entered in Block 20, if different from Report)

18. SUPPLEMENTARY NOTES

19. KEY WORDS (Continue on reverse side if necessary and identify by block number)

Numerical Modelling
Finite Element Simulation
Plasmapause
Magnetospheric Convection
Kp - Correlations
Auroral Ionosphere

20. ABSTRACT (Continue on reverse side if necessary and identify by block number)

The development of computational schemes for numerical modelling of the plasmapause and the aurorally-induced plasma density gradients is described. Variations in location of the equatorial plasmapause are simulated using computer-generated maps representing an ensemble of test particles evolving under co-rotational and convection electric fields. The model has been used to estimate the Transition Time (T_p) from one stable, equilibrium plasmapause configuration to another and to → next page

DD FORM 1 JAN 73 1473 EDITION OF 1 NOV 65 IS OBSOLETE

sub p

Unclassified

SECURITY CLASSIFICATION OF THIS PAGE (When Data Entered)

40 6311

Block 20

sub pp

reproduce Disturbance Scenarios wherein the hour-by-hour changes in plasmapause location at a given local time [L_{pp}(LT)] associated with specified variations in geomagnetic activity are followed.

Modelling of the temporal variations observed in the vertical distribution of plasma in the auroral ionosphere is accomplished using the Finite Element Simulation (FES) scheme. The one dimensional version of this computational technique in operation now incorporates vertical diffusion, gravitational drift and all pertinent chemical reactions.

The results of calculations using both models show that plasma transport effects either dominate or at least significantly contribute to the spatial and/or temporal characteristics of the plasma density feature in question.

CONTENTS

Acknowledgement..... v

Chapter 1. Introduction 1

Chapter 2. Simulation of Plasmapause Dynamics 3

Chapter 3. Finite Element Simulation Applied to the Auroral Ionosphere 25

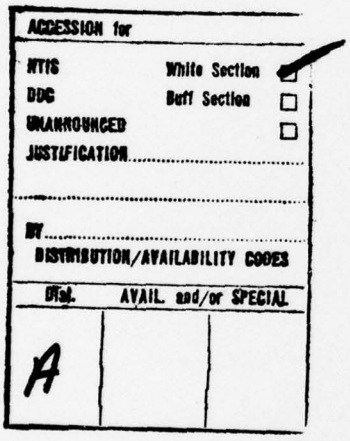

ACKNOWLEDGEMENT

We wish to express our appreciation to Dr. P.J.L. Wildman of AFGL for his help in obtaining and interpreting the ISIS satellite data used in this study, and for many helpful suggestions throughout the course of the investigations. We also wish to acknowledge Ms. R.C. Sagalyn of AFGL for her continued interest and support in these studies. We thank Mr. Louis York of the Astronomy Department, Boston University, for providing valuable help in formulating early versions of Program MAGCON, and Ms. J.L. Mendillo for kindly furnishing the computer graphics routine in MAGCON.

I. INTRODUCTION

This report describes the use of computer simulation techniques to carry out numerical modelling of dynamical properties associated with ionospheric and plasmaspheric boundaries. Two specific cases are dealt with: (1) changes in the equatorial plasmapause location during periods of geomagnetic activity, and (2) the effects of vertical plasma diffusion upon aurorally-induced ionization enhancements at ionospheric heights. For the former case, a scheme was developed whereby changes in magnetospheric convection patterns could be related to plasmapause variations by using computer generated "maps" of an ensemble of equatorial "test particles" to define equilibrium and non-equilibrium configurations of the plasmapause. For the latter case, finite element simulation (FES) techniques were used to construct a one-dimensional model of the temporal evolution of ionospheric plasma produced by energetic particles as found, for example, beneath the magnetospheric cusps or near the poleward wall of the F-region trough. In both cases, the results obtained show that plasma transport effects either dominate or at least significantly contribute to the spatial and/or temporal characteristics of the feature in question.

In Chapter 2, our magnetospheric-convection-dominated model for the formation of the plasmasphere is described. Calculations of convection effects in the equatorial plane are used to address two aspects of time-dependent plasmapause dynamics: (1) the

Transition Time from one stable, equilibrium plasmapause configuration to another, and (2) Disturbance Scenarios, i.e., simulations of the hour-by-hour change in the plasmapause location on the nightside associated with specific variations in geomagnetic activity.

In Chapter 3, we describe the development of a computational scheme based on the Finite Element Simulation technique for handling particle-produced ionization at high latitudes. Initial results obtained by applying a one-dimensional version of this computational scheme to the cusp-related electron density enhancements on the dayside are also presented.

2. SIMULATION OF PLASMAPAUSE DYNAMICS

2.1 Background and Physical Assumptions

Most of the fundamental theoretical studies of the origin and behavior of the equatorial plasmapause (e.g., Nishida, 1966; Brice, 1967; Kavanagh et al., 1968) deal with the application of magnetospheric convection patterns originally suggested by Axford and Hines (1961) to the classic plasmapause geometry reported by Carpenter (1966). The notion of a contracting plasmapause due to enhanced convection patterns during periods of increased geomagnetic activity is now a widely accepted view, and is, in fact, the scheme generally said to explain why statistical results for the plasmapause location (L_{pp}) vs. an index like Kp seem to provide reasonable descriptions of average behavior (Rycroft and Thomas, 1970; Kohnlein and Raitt, 1977). Yet, these simple statistical patterns of L_{pp} vs. Kp are not expected to provide an actual description of the time dependence of plasmapause changes during a specific storm's Kp-scenario. The real plasmapause cannot adjust instantaneously to a new configuration for each Kp step, and within a given Kp interval, the L_{pp} position must be a function of previous magnetic history.

The concept of continuously monitoring the plasmapause location via ground-based or satellite techniques is not a very realistic possibility. Whistler measurements from a fixed site sample a family of field lines, but the measurements are obviously fixed to the Earth's rotating frame of reference and there-

fore only one local time sector is observed at a time. Satellite measurements in or near the equatorial plane offer the best method of determining L_{pp} as a function of local time; due to the need to sample both in the radial and azimuthal directions, a single equatorial satellite does not readily provide good L_{pp} time histories. By far the easiest scheme would be to determine the plasmapause signature at ionospheric heights where several high inclination satellites could provide L_{pp} vs local time morphologies. However, specifying the plasmapause signature in the F-region is not a widely agreed upon concept. At various times, clear L_{pp} signatures in the topside ionosphere appear as (1) an abrupt increase in the H^+/O^+ transition height (i.e., the "light ion trough"), (2) a plasma temperature peak or (3) a steep total ion gradient (i.e., an electron density ledge). The various altitude and latitude characteristics of the quiet-time trough have recently been reviewed by Mendillo and Chacko (1977). In testing a numerical simulation scheme for specific storm-time scenarios (see section 2.2), we decided to rely upon characteristic (3) above, that is, we attempted to reproduce satellite probe determinations of the trough/plasmapause location in the topside F-region ($h \simeq 800 - 3200$ km). The studies carried out by Bewersdorff and Sagalyn (1972) and Wildman et al. (1976) support the view that during periods of increased geomagnetic activity, the steep equatorward edge of the topside plasma trough is probably a good indicator of the plasmapause location.

In developing a model for plasmaspheric dynamics, we assume a completely convection-dominated scheme. By neglecting ionospheric replenishment of the plasmasphere, we limit our results to nighttime effects and to simulation times not much longer than the co-rotation period (24 hours). Both constraints again seem reasonable for periods of increasing geomagnetic activity.

The magnetospheric convection code developed (called Program MAGCON) relies upon computer-generated (i.e., CALCOMP) "maps" of an ensemble of plasmaspheric "test particles" to define equilibrium and transitional configurations of the plasmapause. The model was used to address two specific aspects of plasmaspheric dynamics:

(1) The Transition Time (Tp) from one stable, equilibrium plasmapause configuration to another.

(2) Disturbance Scenarios, i.e., the hour-by-hour changes in the plasmapause location at a given local time ($L_{pp}(LT)$) associated with specified variations in geomagnetic activity.

All of the model studies carried out used the geometry and electric field configurations depicted in Figures 1 and 2 (Mendillo, 1973; Mendillo and Papagiannis, 1971). For any given test particle at a specified local time and L-value, the instantaneous motion of the particle is assumed to be given by $W = (E \times B)/B^2$, where E is the resultant electric field due to co-rotation (E_{ROT} directed radially inward) and convection (E_{DD} directed from dawn to dusk), and B is the dipole field strength in the equatorial plane. A "fluid" of particles is followed by

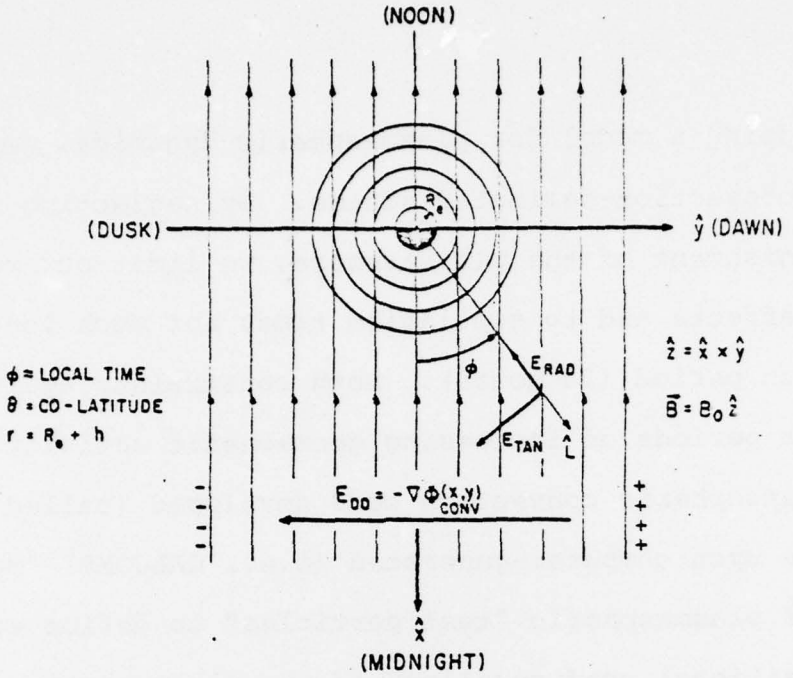

Figure 1. Equatorial Cross-Section of the Magnetosphere ($\theta = 90°$). Concentric rings give unit L-shells, arrows in the $-\hat{x}$ direction give the $\vec{E} \times \vec{B}$ flow lines resulting from the dawn-dusk electric field $-E_{DD}\,\hat{y}$

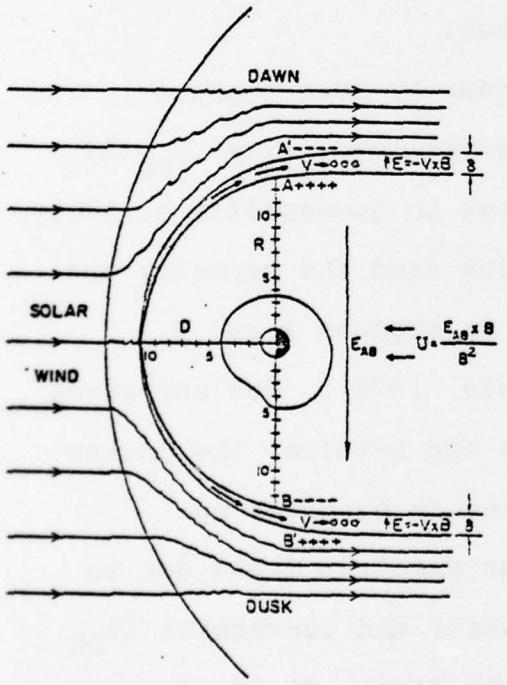

Fig. 2. An equatorial cross section of the magnetosphere. Solar-wind-induced polarization charges at A and B set up the dawn-dusk electric field E_{AS}, which drives the convective motions of plasma from the tail. The plasmapause, shown in the center of the figure, bulges near the dusk meridian to 5 R_E.

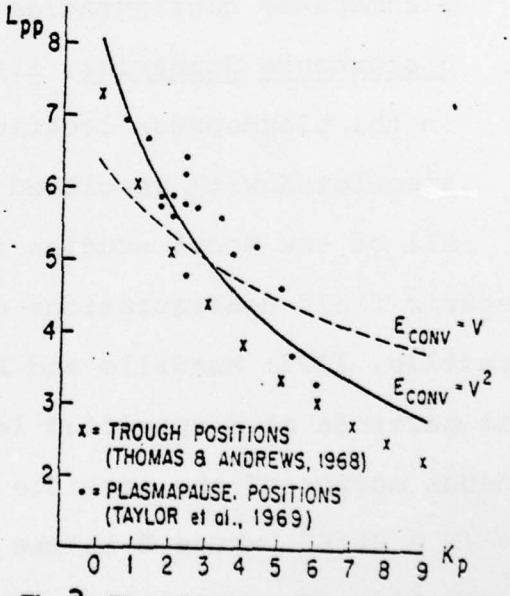

Fig. 3. The solid curve gives the radial behavior of the plasmapause at dusk (L_{pp}) versus Kp from equations 18 and 20 of the model presented. The dashed curve represents the linear L_{pp} dependence suggested by *Vasyliunas* [1968]. The crosses show the behavior of the ionospheric trough at 1800 LT from *Thomas and Andrews* [1968]; the dots are H^+ plasmapause positions near 2400 LT from *Taylor et al.* [1969].

keeping track of all the individual motions using a 10 minute time step. The initial distribution of particles was taken to be circular, with a particle at each ½ L-value from L = 1.5 to 5.5, and spaced every 15 minutes of local time. A total of 864 individual points are therefore available to define subsequent transformations.

2.2. Simulation of Plasmapause Transition Times (Tp)

For a given dawn-to-dusk electric field (assumed to be temporally and spatially constant), a unique plasmapause exists (Kavanagh et al., 1968; Chen, 1970) which defines the boundary between plasma particles which share in the co-rotational field associated with the earth and those which are lost due to magnetospheric convection. The shape of the resultant plasmapause for such a case is the familiar "tear-drop" described by Chen (1970). Thus, our initial circular distribution of particles becomes distorted into a "tear-drop" configuration due to the E_{DD} field. It typically takes about 30 hours of simulation time for a stable configuration to develop, i.e., the remaining fluid particles (perhaps 50 to 75% of the original number) are trapped in motion about the Earth in a region defined by the appropriate theoretical "tear-drop" plasmapause (see Figure 6 in next section). Given this equilibrium plasmapause, we are interested in subsequent transformations caused by a stronger E_{DD} field. Clearly, the new plasmapause position is known in advance since it depends only on the new value of E_{DD}. The actual time it takes to go from one "tear-drop" to another is not known, and thus program

MAGCON lends itself nicely to this type of "dynamic calculation".

In an earlier work (Mendillo and Papagiannis, 1971) we derived an expression for the dependence of the magnetospheric electric field (E_{DD}) on the solar wind speed and related the results to plasmapause changes at 1800 LT through the Kp index (see Figure 3). Using this model for E_{DD} vs. Kp, we computed the set of 10 equilibrium "tear-drop" plasmapause configurations for Kp = 0 to 9. These are plotted on LT/L-value grid in Figure 4, and tabulated values of selected parameters are given in Table 1.

As can be seen from Figure 4, the largest changes in L_{pp} as Kp increases occur in the dusk sector. While the total range of L_{pp} values experienced near 1800 LT seems consistent with available data (see Figure 3), the rather low L_{pp} values at 00 LT and 06 LT suggest that the simple "tear-drop" model, while qualitatively giving the correct dawn - dusk asymetry, does not hold up to quantitative comparisons with real data at all local times. This "improper shape" of the plasmapause will be discussed in a later report. For the present purpose of obtaining estimates of Transition Times (Tp) for the plasmapause configuration associated with one Kp to that associated with another, we decided to use the existing tear-drop configurations.

In operationally computing Tp (say from Kp = 1 to 3), the ensemble of particles occupying the Kp = 1 tear-drop experiences some "peeling-off" in the 12-18 LT sector and compression effects on the nightside. Particles are considered to be lost if they

EQUILIBRIUM PLASMAPAUSE POSITIONS FOR $E_{DAWN/DUSK} = f(K_P)$

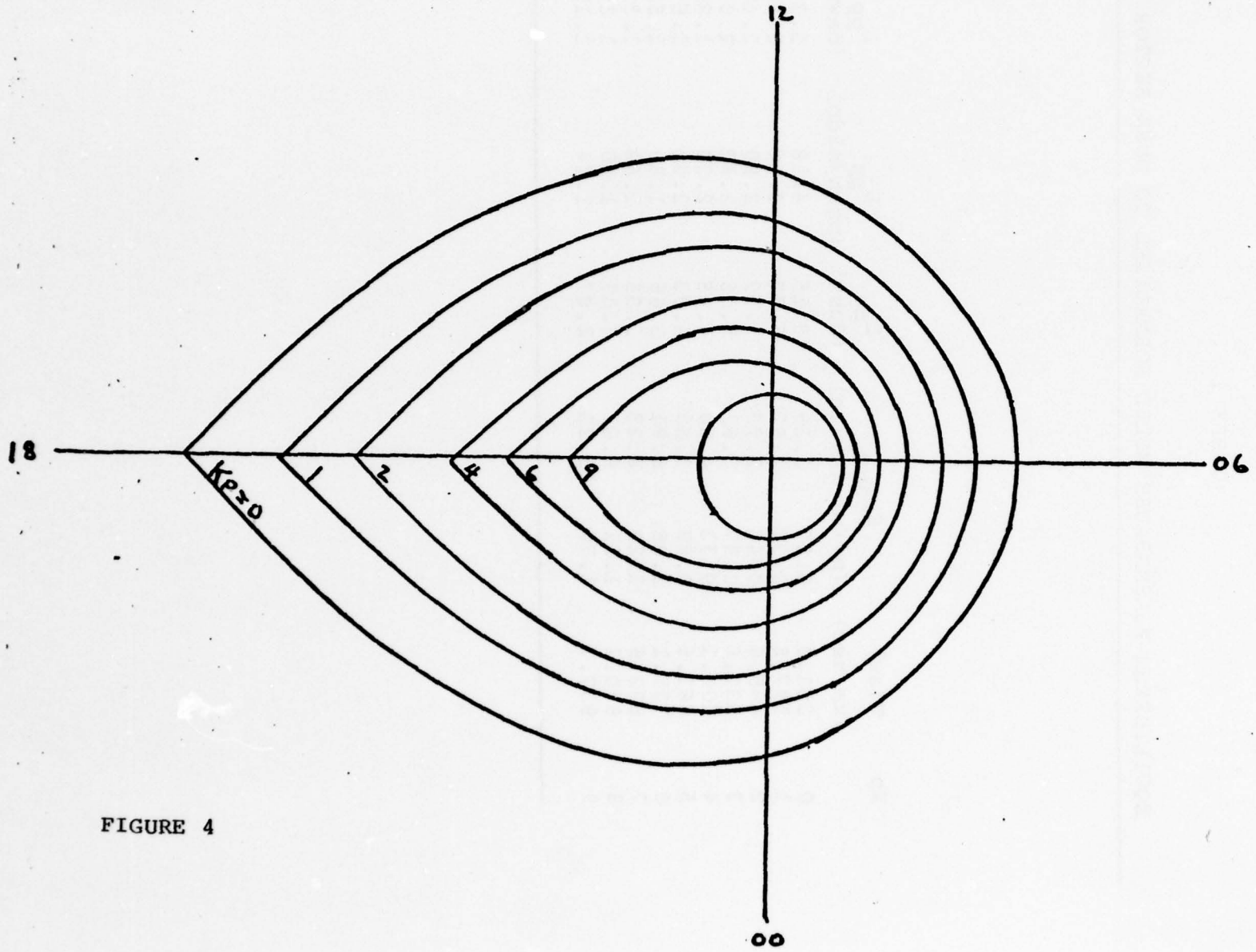

FIGURE 4

TABLE 1

EQUILIBRIUM PLASMAPAUSE MODEL NORMALIZED TO DUSK SECTOR

Kp	V(sw) (km/sec)	E_{conv} (mv/m)	E_{conv} (kv/re)	L_{pp} (dusk)	L_{pp} (noon/midn)	L_{pp} (dawn)
0	330.0	0.22	1.39	8.16	4.08	3.38
1	397.5	0.32	2.02	6.77	3.38	2.80
2	465.0	0.43	2.76	5.79	2.89	2.40
3	532,6	0.57	3.62	5.05	2.53	2.09
4	600.1	0.72	4.60	4.48	2.24	1.86
5	667.6	0.89	5.69	4.03	2.02	1.67
6	735.1	1.08	6.91	3.66	1.83	1.52
7	802.6	1.29	8.23	3.35	1.68	1.39
8	870.2	1.52	9.67	3.09	1.55	1.28
9	937.7	1.76	11.23	2.87	1.44	1.19

convect to an L-value greater than the new L_{pp} (18 LT) value, or move to L = 1. We define "100% equilibrium" to occur when literally all the particles capable of being lost are lost. Similarly, the 25%, 50%, and 90% equilibrium times are the time intervals it takes for 25%, 50%, and 90% of the particles going to be lost are lost, respectively. A set of such Transition Time results are displayed in Table 2. Note that the format gives the Tp(25%), Tp(50%), Tp(90%), and Tp(100%) times for transformations of Kp (initial) to Kp (final). In examining the Tp(100%) results, one can see that Tp is large (≃30 hours), independent of whether the Kp step is small (i.e., Kp = 0→1, 1→2, 0→2, 6→8) or large (Kp = 0→6, 1→5, 2→8, 5→9). This results from the rigid constraint that all points to be lost are lost. Thus, a point which just escaped being "peeled-off" near 1500 LT rotates (at a speed less than the co-rotational speed) around the nightside and is ultimately peeled-off during the following dayside transit. It would appear that there are always points which fall into this category (or linger for a very long time near the stagnation point at 1800 LT), and thus a diurnal (≃30 hr.) time scale results for the Tp(100%) condition.

Waiting for the "last point to be lost" clearly seems to be too rigid a condition. Since we are more interested in the plasmapause location on the nightside (where its relationship to the trough may best exist), and since the nightside sunward convection affects the L_{pp} (18→06 LT) values more directly, we view the

K_p FINAL \ INIT.	0	1	2	3	4	5	6
1	9 | 12 20 | 29						
2	6 | 10 19 | 31	8 | 11 23 | 32					
3			8 | 11 20 | 28				
4			5 | 9 20 | 36	11 | 16 19 | 27			
5		3 | 6 17 | 35			10 | 11 19 | 27		
6	1 | 4 15 | 29				6 | 10 22 | 32	9 | 13 18 | 22	
7							15 | 16 21 | 25
8			4 | 6 16 | 30				9 | 10 18 | 29
9						6 | 8 18 | 30	

LEGEND:

$\Delta N \equiv$ # OF PARTICLES LOST FROM PLASMASPHERE DURING K_p INCREASE

T_p = TIME REQUIRED FOR THE INDICATED PERCENTAGE OF ΔN TO OCCUR (HRS.)

T_p(25%)	T_p(50%)
T_p(90%)	T_p(100%)

TABLE 2. PLASMAPAUSE TRANSITION TIMES.

50% equilibrium values of Tp to be more representative of the time lag associated with a Kp/plasmapause transition. An examination of the Tp(50%) results in Table 2 reveals that Tp becomes smaller the larger the change in Kp. Thus, when $\Delta Kp = 1$, Tp = 11-16 hours, for $\Delta Kp = 2$, Tp = 9-10 hours, for $\Delta Kp = 4$, Tp = 6-8 hours, and for $\Delta Kp = 6$, Tp = 4-6 hours. This seems to be a consistent relationship for all Kp levels and may be described in the average by the curve given in Figure 5. The results suggest that if statistical studies relating the nighttime plasmapause to Kp are to be used as predictors of actual boundary locations, an appropriate time lag should be used dependent upon the actual increase in Kp encountered.

2.3. Simulation of Plasmapause Disturbance Scenarios.

The second aspect of our investigations using Program MAGCON was an attempt to simulate actual "disturbance scenarios" via the model and relate the changes observed to actual measurements (ISIS-1 data furnished by AFGL) and past statistical studies. We selected several case study periods for simulation, the choices being determined by: (1) availability of AFGL data, (2) the desire to have well-defined disturbance periods following a period of steady activity (i.e., Kp = 1,2 or 3 for nearly 24 hours), and (3) the realization that only the 2200-0600 LT period lends itself to our modelling capabilities.

Before proceeding we had to contend with the fact that the equilibrium plasmapause contours given in Figure 4 do not give "reasonable" L_{pp} values in the pre-midnight to dawn sector. As

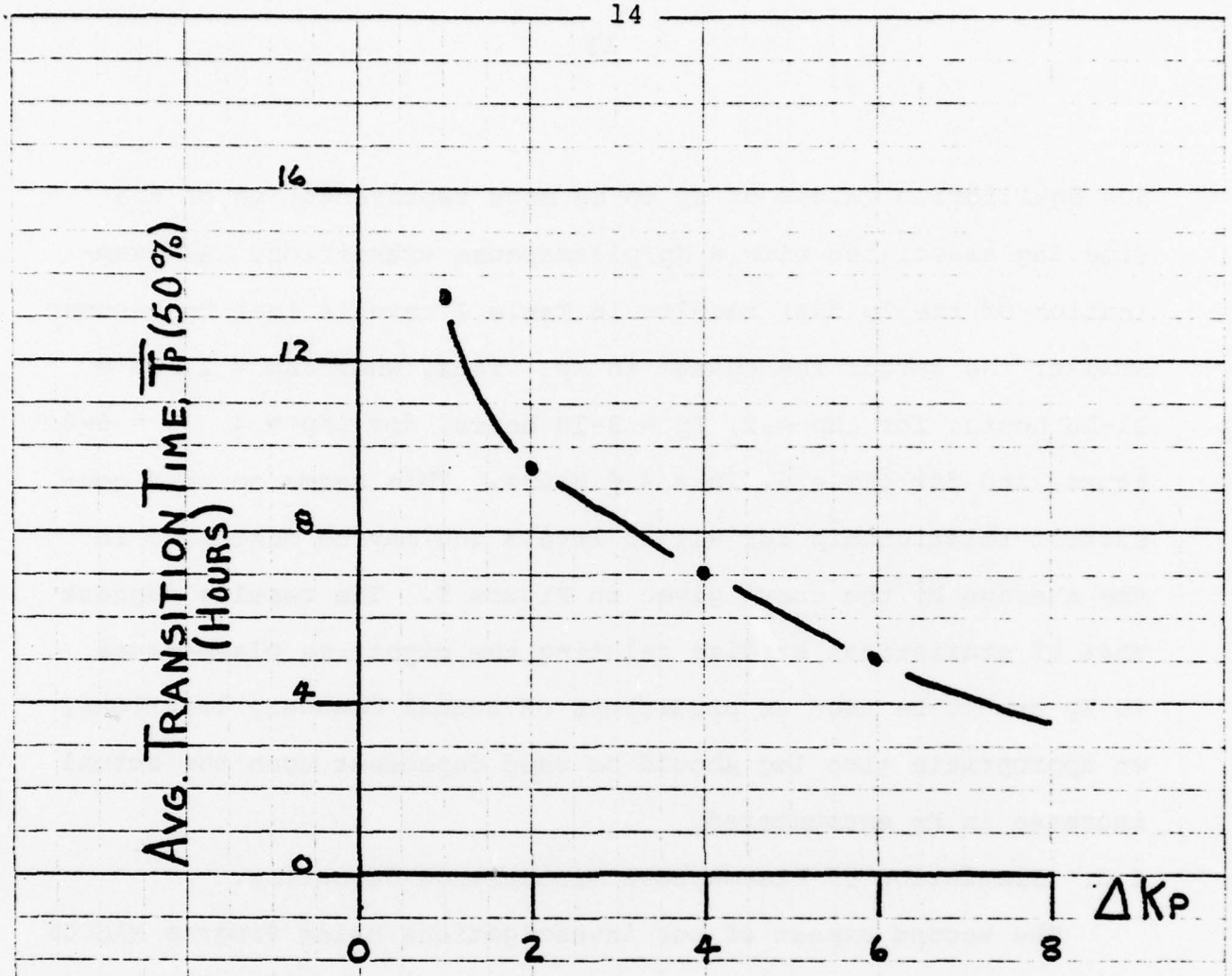

ΔKP	TP(50%)	$\overline{T_P}$(50%)
1	11-16	13.5
2	9-10	9.5
4	6-8	7.0
6	4-6	5.0

FIGURE 5

mentioned earlier, the "tear-drop" shape gives too severe a dawn-dusk asymmetry. The 50% decrease in L_{pp} from 1800 LT to 00 LT is not reflected in actual data, and thus we decided to re-normalize our quadratic E_{DD} vs. Kp relation (as derived in Mendillo and Papagiannis (1971) for the 1800 LT sector) to actual L_{pp} (00 LT) AFGL/ISIS observations. An examination of the existing data base revealed that L_{pp} (00 LT) = 5 for K_p = 2, and thus this normalization point was chosen for the E_{DD} vs. Kp relation, rather than the L_{pp} (18 LT) = 5 for Kp = 3 used previously. The new set of reduced electric field values and consequent L_{pp} locations are given in Table 3.

To illustrate the procedure, consider the storm period of 21-22 April, 1971. Prior to 1200 UT, magnetic activity was steady for nearly 9 hours, with Kp = 2. From 1200 UT on, Kp (a 3-hour index) varied as follows: 3, 4, 5, 7, 5, 3, 2. To follow the nightside L_{pp} variations associated with this scenario, we first used our simulation program to generate the equilibrium ("tear-drop") particle distribution appropriate to the t=0 point of the scenario. Thus, the initial circular distribution of particles was allowed to evolve to the case: 12:00 UT on 21 April 1971, Kp = 2 (Figure 6). The electric field model was then used to input new E_{DD} fields in concert with the observed Kp variation. Computer generated plots of the modified particle distributions were made at hourly intervals, and the L_{pp} boundary values for the LT sector in question were scaled from the plots (see Figure 7 for sample outputs 2, 9, 12, and 20 hours into the simulation).

TABLE 3

EQUILIBRIUM PLASMAPAUSE MODEL NORMALIZED TO MIDNIGHT SECTOR

Kp	V(sw) (km/sec)	E_{conv} (mv/m)	E_{conv} (kv/re)	L_{pp} (dusk)	L_{pp} (noon/midn)	L_{pp} (dawn)
0	330.0	0.07	0.46	14.09	7.05	5.84
1	397.5	0.10	0.66	11.70	5.85	4.85
2	465.0	0.14	0.91	10.00	5.00	4.14
3	532.6	0.19	1.19	8.73	4.37	3.62
4	600.1	0.24	1.51	7.75	3.87	3.21
5	667.6	0.29	1.87	6.97	3.48	2.87
6	735.1	0.36	2.27	6.33	3.16	2.62
7	802.6	0.42	2.70	5.79	2.90	2.40
8	870.2	0.50	3.18	5.34	2.67	2.21
9	937.7	0.58	3.69	4.96	2.48	2.05

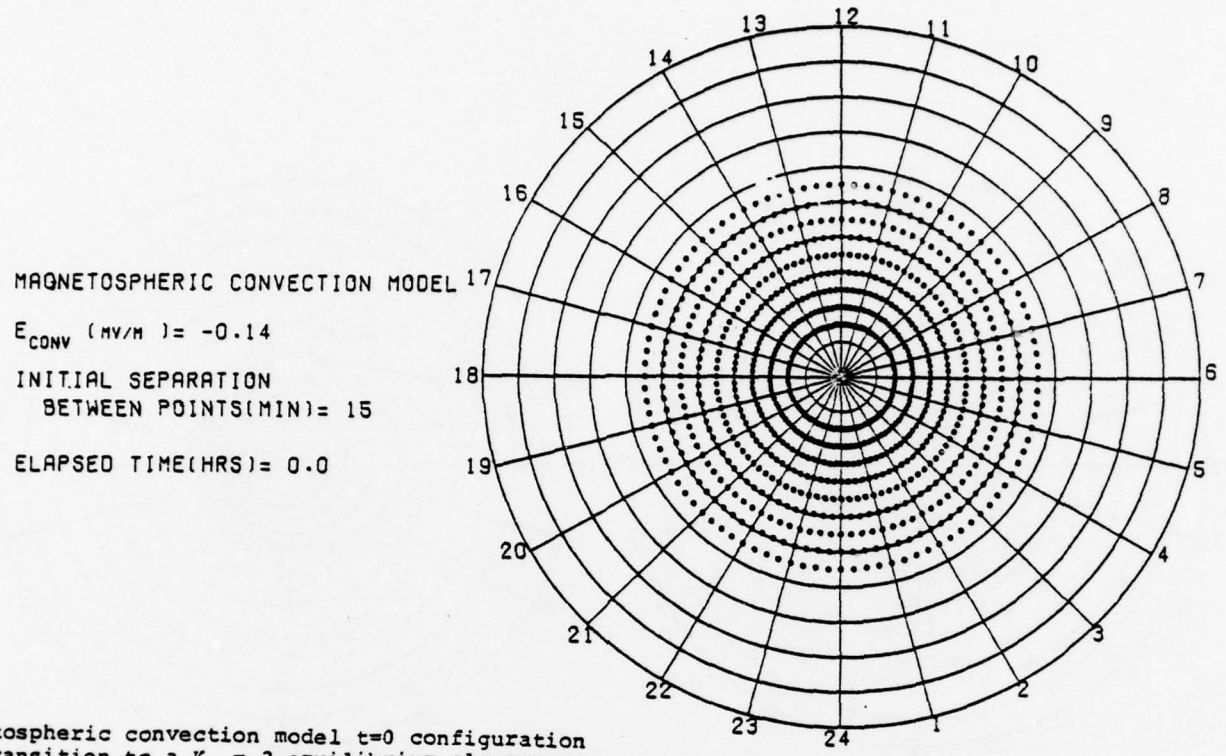

Magnetospheric convection model t=0 configuration for transition to a K_p = 2 equilibrium plasmapause (E_{DD} = 0.14 mv/m).

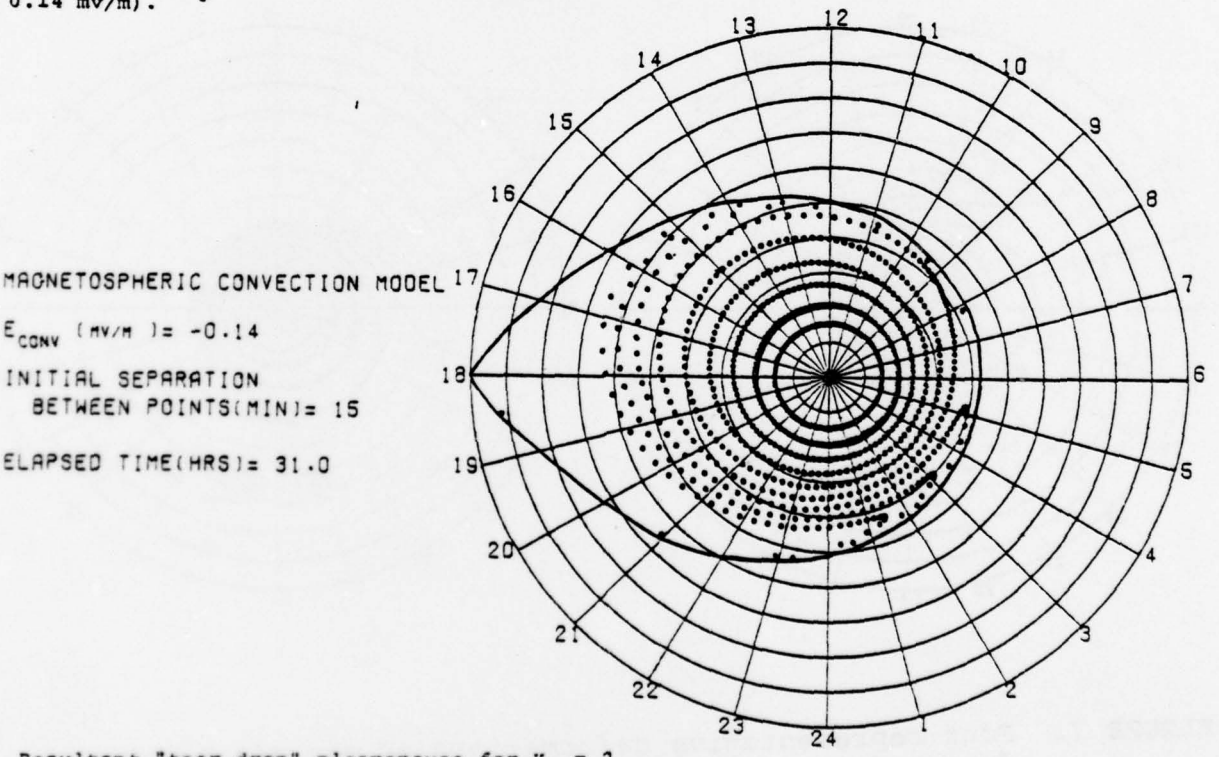

Resultant "tear drop" plasmapause for K_p = 2 after 31 hours simulation time. This equilibrium boundary represents the t=0 point for a K_p scenario beginning with K_p = 2 (e.g., at 1200 UT on 21 April 1971).

FIGURE 6

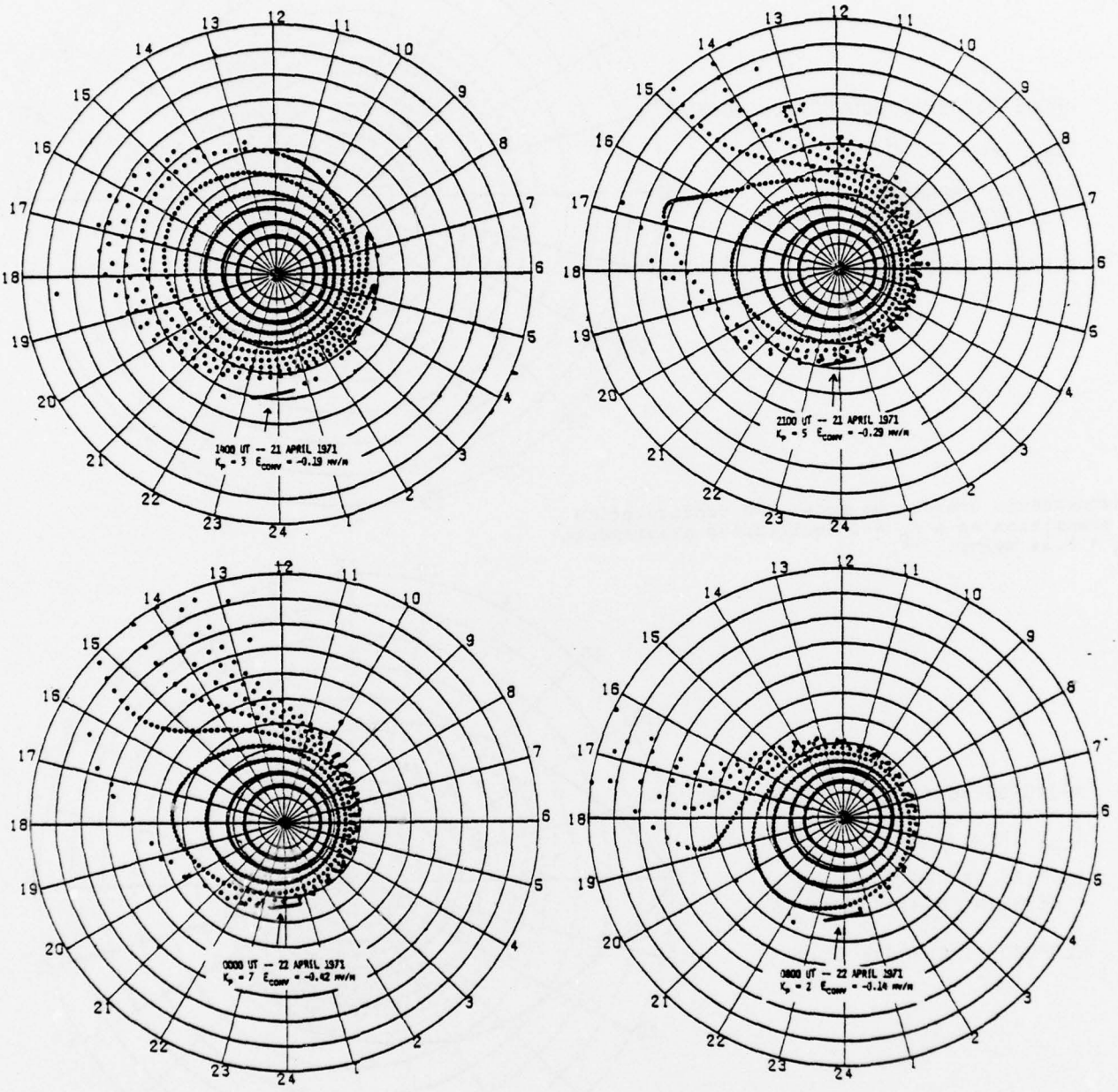

FIGURE 7. Four representative deformations of the plasmasphere depicted in Figure 8 at t=2,9,12 and 20 hours into the K_p scenario for 21-22 April 1971. The arrows indicate the L_{pp} boundary segments as defined by the particles at 23:45 LT.

For this particular scenario, we examined the 2345 LT values in order to compare the model's predictions with ISIS-1 in-situ probe data for the equatorward edge of the total ion trough in the topside F-region (Wildman et al., 1976). The results are given in Figure 8, together with the "statistical predictions" of the L-value of the plasmapause using the relation given by Rycroft and Thomas (1970).

In examining the results, there are several features to note:

(1) The trough's equatorward edge (measured high in the F-region) is probably a better indicator of the plasmapause location during disturbed times than during quiet periods. Thus, at the t=0 point of the scenario, the difference between the data and the model is the largest.

(2) As the storm progresses (in this case, rather smoothly from Kp = 3→4→5→8), the steady contraction of the plasmapause is reproduced. The statistical results of Rycroft and Thomas (1970) appear as discontinuous jumps every 3 hours (the Kp interval); they also tend to agree with the observed behavior.

(3) Following the storm maximum, i.e., after 00 LT on 22 April 1971, the Kp transition 5→3→2 causes a gradual recovery of the plasmapause to higher L-values. There is a definite "sluggishness" built into the model arising from the previously high Kp values. This ability to take previous magnetic history into account is in sharp contrast to the statistical predictions which show instantaneous adjustments to higher L_{pp} values.

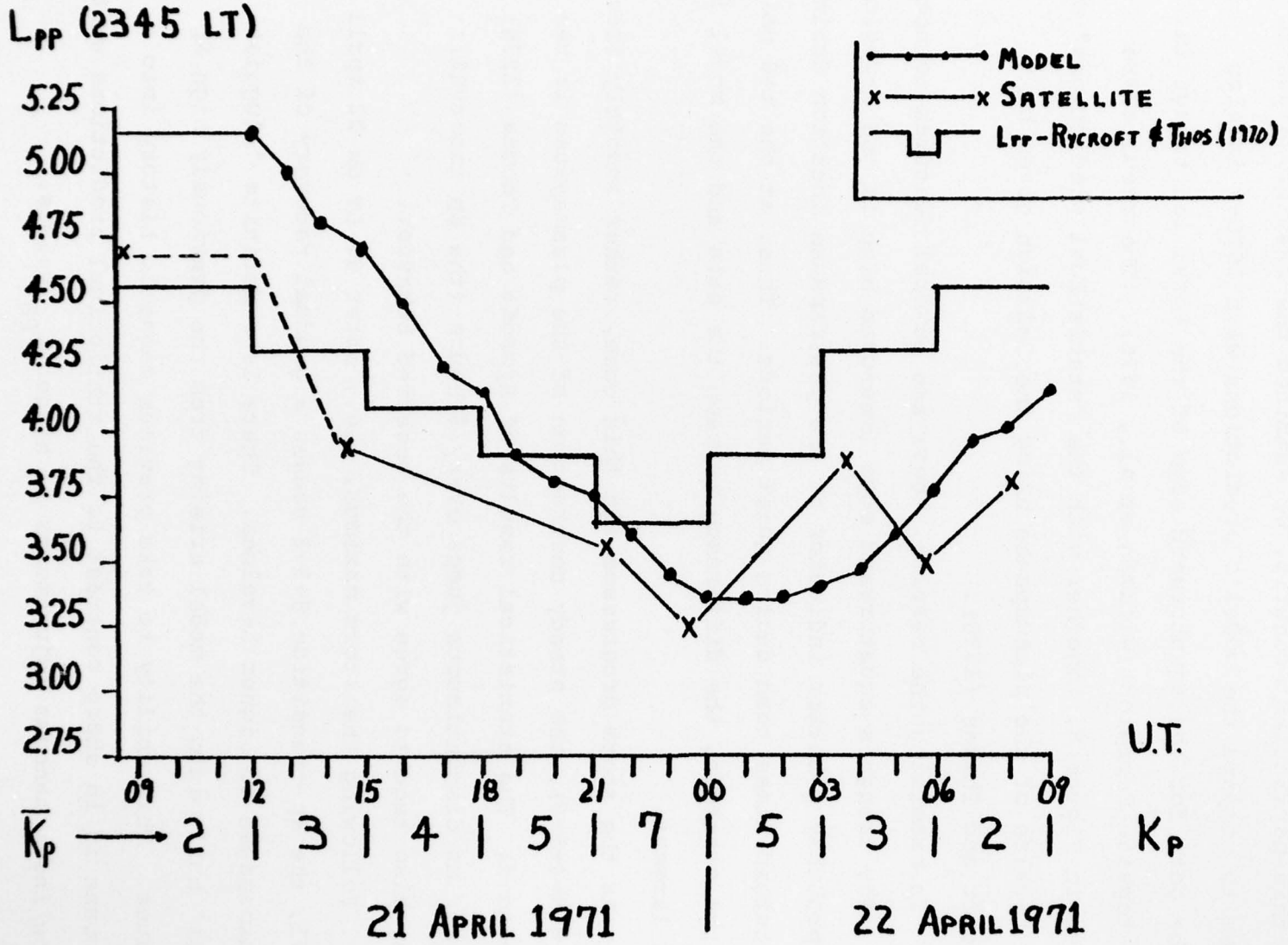

FIGURE 8

Overall Model Results for the K_p scenario of 21-22 April 1971, shown in comparison to ISIS probe data giving the equatorward edge of the F-region trough, and statistical results of Rycroft and Thomas (1970).

We have tested this procedure for other Kp scenarios and find the "sluggishness" of the model to be a major asset for both intensification effects (e.g., Kp = 1→5) and recovery patterns.

Figure 9 gives a second example for which frequent satellite data were available. The period considered was a large and protracted storm, giving us the opportunity to test the modelling scheme for an extended period of relatively high geomagnetic activity. The model predictions are again remarkably consistent with the satellite data.

In summary, our numerical simulation studies of magnetospheric convection, as related to plasmapause dynamics, have yielded some quantitative conclusions about plasmapause transition times and ΔKp (summarized in Figure 5), and definite evidence that a relatively simple physical model for a convection-dominated plasmapause can be used to simulate nightside dynamics effects (as evidenced in Figures 8 and 9).

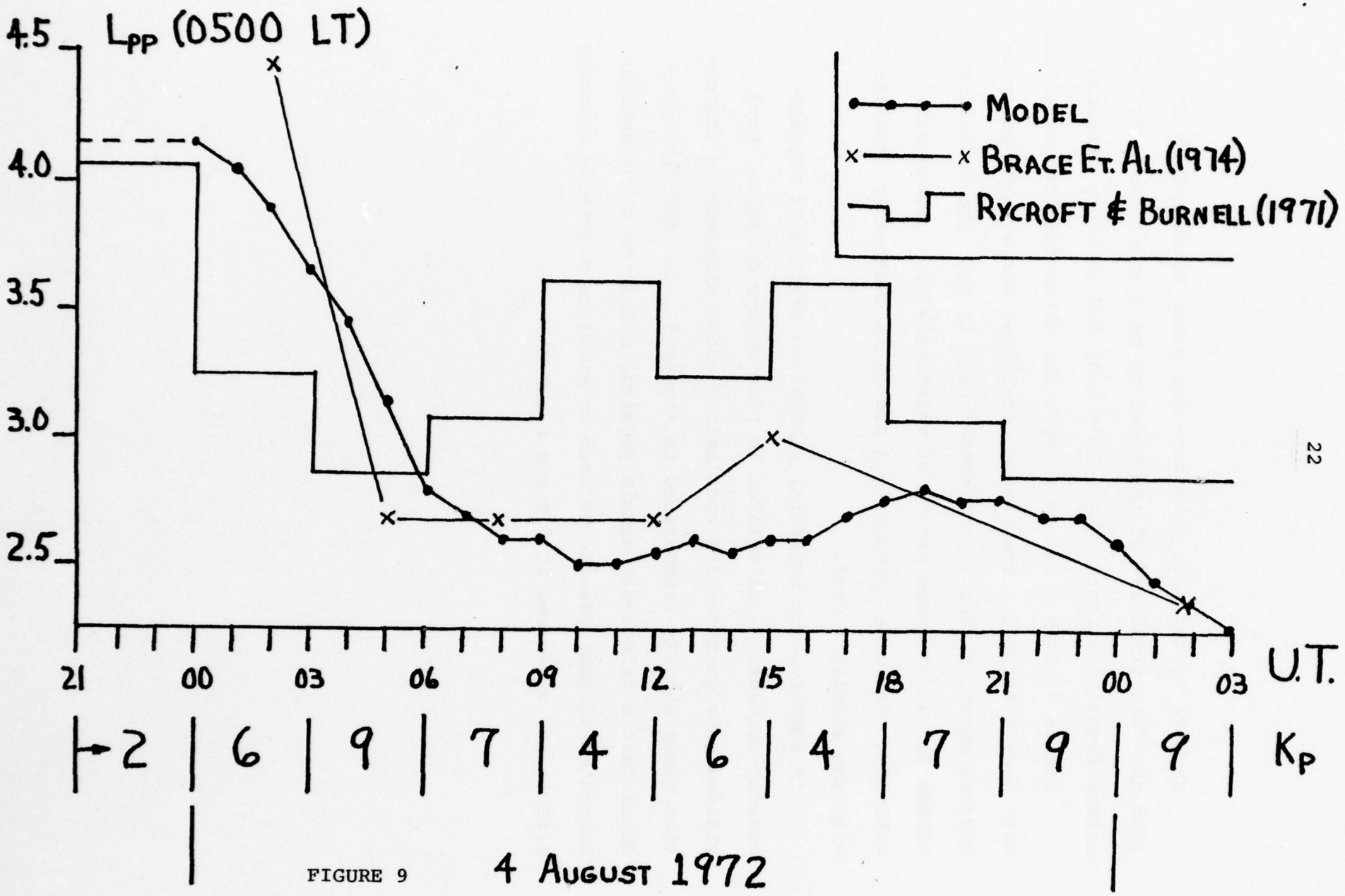
4.5
4.0
3.5
3.0
2.5
L_{PP} (0500 LT)
MODEL
BRACE ET. AL. (1974)
RYCROFT & BURNELL (1971)
21
00
03
06
09
12
15
18
21
00
03
U.T.
2
6
9
7
4
6
4
7
9
9
K_P
4 AUGUST 1972

FIGURE 9

REFERENCES

Axford, W.I. and C.O. Hines, A Unifying Theory of High-Latitude Geophysical Phenomena and Geomagnetic Storms, Can. J. Phys., 39, 1433, 1961.

Bewersdorff, A.B. and R.C. Sagalyn, Spatial and Temporal Variations of the Thermal Plasma Between 3000 and 5700 Kilometers at L = 2 to 4, J. Geophys. Res., 77, 4734, 1972.

Brice, N.M., Bulk Motion of the Magnetosphere, J. Geophys. Res., 72, 5193, 1967.

Carpenter, D.L., Whistler Studies of the Plasmapause in the Magnetosphere, 1, Temporal Variations in the Position of the Knee and Some Evidence on Plasma Motions Near the Knee, J. Geophys. Res., 75, 693, 1966.

Chen, A.J., Thermal and Quasi-Energetic Plasma Flow in the Magnetosphere - A Theoretical Study, Ph. D. Dissertation, Rice Univ., Houston, Texas, 1970.

Kavanagh, Jr., L.D., Freeman, Jr., J.W. and A.J. Chen, Plasma Flow in the Magnetosphere, J. Geophys. Res., 73, 5511, 1968.

Kohnlein, W., and W.J. Raitt, Position of the Mid-Latitude Trough in the Topside Ionosphere As Deduced From ESRO 4 Observations, Planet. Space Sci., 25, 600, 1977.

Mendillo, Michael, Magnetospheric Convection at Ionospheric Heights, Tech. Report AFCRL-73-0358, AFCRL, Bedford MA, 1973.

Mendillo, Michael and C.C. Chacko, The Base Level Electron Density Trough, J. Geophys. Res., 82, 5129, 1977.

Mendillo, Michael and Michael D. Papagiannis, Estimate of the Dependence of the Magnetospheric Electric Field on the Velocity of the Solar Wind, J. Geophys. Res., 76, 6939, 1971.

Nishida, A., Formation of Plasmapause, or Magnetospheric Plasma Knee, By the Combined Action of Magnetospheric Convection and Plasma Escape From the Tail, J. Geophys. Res., 71, 5669, 1966.

Rycroft, M.J. and J.O. Thomas, The Magnetospheric Plasmapause and the Electron Density Trough at the Alouette I Orbit, Planet. Space Sci., 18, 65, 1970.

Wildman, P.J.L., Sagalyn, R.C. and M. Ahmed, Structure and Morphology of the Main Plasma Trough in the Topside Ionosphere, Proc. COSPAR Sym. Geophys. Use of Sat. Beacon Obs., M. Mendillo (ed), Boston University, Boston, MA, June 1976.

3. FINITE ELEMENT SIMULATION APPLIED TO THE AURORAL IONOSPHERE

Two of the major effects precipitating magnetospheric particles have upon the earth's upper atmosphere are excitation of the auroral spectrum and the production of ionization. While auroral studies have grown into an important discipline in space research (see, for example, the treatise by Akasofu, 1977) the latter effect has attracted only limited attention [Rees, 1963; Banks et al., 1974; Mantas and Walker, 1976] despite its importance in applications to radio wave propagation. The processes controlling the redistribution of particle-generated ionization at high latitudes are many and complex: they stem from chemical reactions, vertical diffusion, heating, $\underline{E}$-fields, neutral winds and related effects.

The purpose of the investigation reported on here has been to develop, as a first step towards a more comprehensive capability, a one-dimensional simulation technique to describe the vertical distribution of electron density in the high latitude ionosphere. The computational procedure adopted is Finite Element Simulation [Balko and Mendillo, 1977]. The FES technique relies on the application of physical and chemical laws, usually in a linearized version, to the system under investigation in the following manner.

The system is divided into a number of convenient cells (labeled i,j,k), using the symmetry of the situation to advantage so as to minimize the number of geometrical parameters.

Each cell is characterized by three types of parameters:

a) Geometrical parameters $\mathcal{G}(i)$, such as the position of the center of a cell, its volume, cross sectional area, surface area, etc.

b) Physical parameters $\mathcal{P}(i)$, such as diffusivity, specific heat, etc.

c) Transport functions $\tau(i)$, such as temperature, concentration, pressure, etc.

$\tau(i)$ is an intensive parameter and the associated extensive parameters, e.g. heat, number of particles, is denoted $Q(i)$. The parameters in group (c) are specified initially, $\tau(i)$ at $t=0$, and then a time interval Δt is chosen over which the calculation is to take place. The choice of Δt is governed by the requirement that it should be small enough to prevent "overshoot" in the calculations.

The heart of the calculation is the set of physical laws which describe changes in the system parameters $\tau(i)$ over the interval $(t, t + \Delta t)$. A general process (m) can be thought of as causing a change $\Delta Q^{m}(i)$ due to the transfer parameter $\tau^{m}(i)$ of cell i. It can be calculated from

$$\Delta Q^{m}(i) = \Omega(i, i+1) \cdot \Lambda(i, i+1) \cdot \Phi(i, i+1)\, \Delta t \quad (1)$$

where Ω, Λ and Φ are functions of the appropriate geometrical, physical and transfer parameters of the system.

$\Delta Q^{m}(i)$ is a change in the extensive parameter corresponding to $\tau^{m}(i)$ and gives the amount of "material" transferred out of

cell (i) by the process m. In the case of molecular diffusion, ΔQ is the number of molecules transported in time Δt, due to concentration differences in the cells. The changes in the transport functions can be obtained from

$$\Delta\tau^m(i) = (\Delta Q^m(i-1) - \Delta Q^m(i))/R^m(i) \qquad (2)$$

This leads to a new $\tau(i)$ at time $t + \Delta t$ which is obtained from all the $\Delta\tau^m(i)$ by

$$\tau(i)_{new} = \tau(i)_{old} + \sum_{m=1}^{M} \nabla\tau^m(i) \qquad (3)$$

where we have assumed (M) independent processes affecting the parameter $\tau(i)$.

The preceding three steps are repeated until t_{max} is reached. The result of the calculation is a profile of the τ parameter as a function of position (cell center) for different times. Note that this is a dynamic simulation calculation so that in order to obtain an equilibrium situation the temporal development has to be simulated until an asymptotic behavior is reached.

<u>One Dimensional Diffusion</u>

Figure 10 represents the simple geometry we have adopted for the problem of vertical diffusion of charged particles in the earth's upper atmosphere ($150 \leq h \leq 1500$ km). For simplicity we assume 1) the earth's magnetic field $B = B\hat{Z}$ and 2) the horizontal cross-sectional area of the cells $A(Z) = A$ = constant. Typically, A = 20 km × 20 km and the total number of cells = 40.

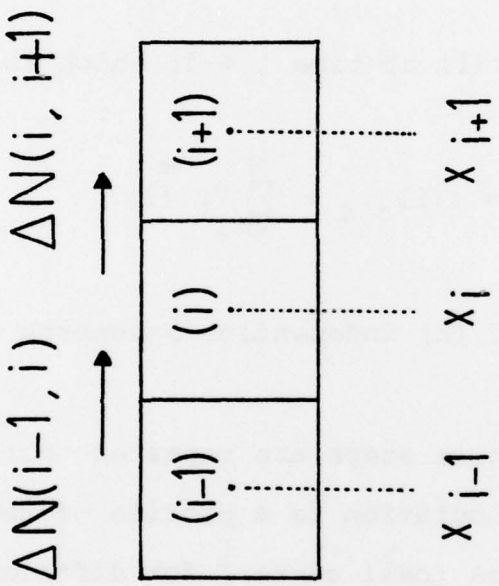

FIGURE 10. CELL GEOMETRY FOR ONE-DIMENSIONAL VERTICAL DIFFUSION.

The number of molecules transferred by diffusion from cell (i-1) to cell (i) during the time interval Δt is given by

$$\Delta N(i-1, i) = \frac{-AD}{\Delta Z(i-1, i)} [C(i) - C(i-1)] \cdot \Delta t \qquad (4)$$

where for cell i the quantity $\Delta N(i-1, i)$ is positive if the particle flux is into the cell. Note that the diffusivity D represents <u>effective</u> diffusivity defined as

$$D = \frac{\ell_i + \ell_{i-1}}{\ell_i/D_i + \ell_{i-1}/D_{i-1}} \qquad (5)$$

where ℓi is the length of the i^{th} cell. C(i) is the concentration of the diffusing species in cell i, $\Delta Z(i-1, i) = Z(i) - Z(i-1)$, separation of centers of cells i and i-1.

Analytically, this expression can be written as a flux from one cell into the other, dependent on the gradient between the two cells. Defining a flux into a cell as positive,

$$F = -D \frac{dC}{dZ}$$

where D is again the diffusion coefficient and F is the number of particles crossing a unit area per unit time between the interface of the two cells, $F = \frac{1}{A} \frac{dN}{dt}$. The concentration change in the ith-cell after diffusive transfer between it and the two adjacent cells i-1 and i+1 is

$$\Delta C_i^D = [\Delta N^D(i-1, i) - \Delta N^D(i, i+1)] \cdot \frac{1}{V_i} \qquad (6)$$

where V(i) is the volume of the ith cell. This is a special

case of equation (2) where the parameter $R^m(i)$ is simply the volume of the ith cell. The new concentrations at time $t + \Delta t$ are

$$C_i(t + \Delta t) = C_i(t) + \Delta C_i^D \tag{7}$$

This operation is performed for all the N cells in the system and is repeated n times for subsequent time intervals until the maximum required time $t_{max} = n\Delta t$ is reached. The calculation step (Δt) need not remain constant over the entire time span t_{max}, but could be changed as the calculation evolves. The result of the calculation is a "concentration profile" of the system as a function of time.

We can now show the correspondence between the above approach and the diffusion equation. Consider the simple case of a homogeneous medium. The concentration change over the time interval Δt as calculated from equations (4) and (6) may be written as

$$\frac{\Delta C_i(t, \Delta t)}{\Delta t} = D \cdot \frac{A}{\Delta Z_i}[C_{i-1} + C_{i+1} - 2C_i] \cdot \frac{1}{V_i} \tag{8}$$

where $V_i = A \cdot \Delta Z_i$ is the volume of cell i and all cells are assumed to have identical cross-sectional areas and linear dimensions. Changing notations to $C_i \rightarrow C(Z)$, $C_{i-1} \rightarrow C(Z-\Delta Z)$, $C_{i+1} \rightarrow C(Z + \Delta Z)$ and taking the limit as $\Delta t \rightarrow 0$ and $\Delta Z \rightarrow 0$ independently, we get

$$\frac{\partial C}{\partial t} = D \frac{\partial^2 C}{\partial Z^2} \tag{9}$$

by the definition of the derivative. We have thus derived the diffusion equation from our two equations of transport in a homogeneous medium.

The next step in building up our simulation of the transport phemomena is to introduce the force field drift term (ΔC_i^F) which, in our case of atmospheric diffusion, arises from the Earth's gravitational attraction. Given an effective drift velocity G_i' between cells (due, in this case, to the gravitational acceleration) the number of molecules transferred from cell (i) to cell (i+1) in the time Δt is given by

$$\Delta N^F(i,i+1) + G_i' \frac{V_i}{\Delta Z_i} C_i \, \Delta t$$

where G_i is calculated the same way as D_i (see equation 5). The change in the concentration of cell i due to this process is

$$\Delta C_i^F = [\Delta N^F(i-1, i) - \Delta N^F(i, i+1)] \cdot \frac{1}{V_i} \qquad (10)$$

Analytically, this change is usually referred to as the 'advection term' in the continuity equation for concentration (C). It gives the time rate of change in C due to drifting spatial gradients in C, i.e.

$$\frac{\partial C}{\partial t} = \bar{v} \cdot \nabla C = v \frac{\partial C}{\partial Z}$$

Following the procedure used with the diffusive term above, we can show that equations (1), (2), (5), (10), in the appropriate limit can be used to derive Smoluchowski's equation for diffusion in a force field .

$$\frac{\partial C}{\partial t} = D \frac{\partial^2 C}{\partial Z^2} + G \frac{\partial C}{\partial Z} \tag{11}$$

for a homogeneous medium.

Finally, for reactive substances we introduce the change in concentration due to chemical reactions. Suppose the diffusing substance reacts with a background constituent whose concentration in cell i is given by C_i^b . The change in concentration of C_i due to reactions of the diffusing material during the time interval Δt is given by

$$\Delta C_i^R = -kC_i \cdot C_i^b \Delta t \tag{12}$$

where k is the chemical reaction rate in units of volume/time.

In summary, if Ci^{α} represents the concentration of substance α ($\alpha = 1,...n_{\alpha}$) in cell i, then the total change in concentration is obtained from

$$\Delta Ci^{\alpha}(t, \Delta t) = \Delta C_{\alpha}^{D},i + \Delta C_{\alpha}^{F},i + \Delta C_{\alpha}^{R},i \tag{13}$$

Computations and Results

Electron density enhancements in the F-region beneath the day side magnetospheric cusp represents a relatively simple case of particle-generated ionization in the earth's upper atmosphere [Chacko and Mendillo, 1977]. We have applied the FES technique sketched in the previous section to this problem. The model incorporates vertical diffusion of O^+ and H^+, gravitational drift and predominant chemical reactions.

Table 4 shows values of the diffusion coefficients we have adopted [Banks and Kockarts, 1973]. Table 5 lists the chemical reactions and their rate coefficients included in the computations.

Figure 11 shows the initial O^+ and H^+ distributions which form part of the input into the program. The lower parts of both profiles as well as the upper part of the H^+ profile represent reasonable but arbitrary values while the upper F-region values for $[O^+]$ are the measured electron densities at 75.5° Corrected Geomagnetic Latitude during quiet periods in December 1971 [Chacko and Mendillo, 1977]. These initial profiles are considered adequate for the purpose of demonstrating the feasibility of the FES scheme in the area of plasma diffusion at high latitudes.

Figure 12 shows the evolution of O^+ and H^+ profiles at the end of 15 minutes as a result of diffusion and the chemical reactions listed above as well as of gravitational drift. Figure 13 represents the vertical O^+ and H^+ distributions at the end of 20 minutes of real time when, in addition to the above processes, in-situ production by soft electrons [Knudsen et al., 1977] was allowed to operate for the last 5 minutes. The fact that the final profiles are well-behaved and quantitatively realistic shows that the FES scheme we have developed can now be utilized to obtain quantitative results in the field of plasma diffusion at high latitudes.

TABLE 4

DIFFUSION COEFFICIENTS

Species	D (cm^2/sec)
O^+-O	$\frac{3.1 \times 10^{17}}{[O]} \frac{T_i^{1/2}}{(1 + T_n/T_i)^{1/2}}$
O^+-O_2	$7.2 \times 10^{15} \frac{T_i}{[O_2]}$
O^+-N_2	$8.5 \times 10^{15} \frac{T_i}{[N_2]}$
O^+-He	$5.6 \times 10^{16} \frac{T_i}{[He]}$
O^+-H	$4.0 \times 10^{16} \frac{T_i}{[H]}$
O^+-H^+	$9.4 \times 10^{7} \frac{T_i^{5/2}}{[H^+]}$
H^+-O	$3.7 \times 10^{16} \frac{T_i}{[O]}$
H^+-O_2	$2.6 \times 10^{16} \frac{T_i}{[O_2]}$
H^+-N_2	$2.5 \times 10^{16} \frac{T_i}{[N_2]}$
H^+-He	$7.8 \times 10^{16} \frac{T_i}{[He]}$
H^+-O^+	$6.9 \times 10^{7} \frac{T_i^{5/2}}{[O^+]}$
H^+-H	$\frac{8.0 \times 10^{17}}{[H]} \frac{T_i^{1/2}}{(1 + T_n/T_i)^{1/2}}$

TABLE 5

CHEMICAL REACTIONS AND THEIR RATES

Reaction	Rate (cm^3/sec)
$O^+ + N_2 \rightarrow N + NO^+$	$1.2 \times 10^{-12}(300/T_n)$
$O^+ + O_2 \rightarrow O + O_2^+$	$2.0 \times 10^{-11}(300/T_n)^{\frac{1}{2}}$
$NO^+ + e^- \rightarrow N + O$	$4.1 \times 10^{-7}(300/T_e)$
$O_2^+ + e^- \rightarrow O + O$	$2.2 \times 10^{-7}(300/T_e)^{0.85}$
$O^+ + H \rightarrow H^+ + O$	$2.5 \times 10^{-11}\ T_n^{\frac{1}{2}}$
$H^+ + O \rightarrow O^+ + H$	$2.3 \times 10^{-11}\ T_i^{\frac{1}{2}}$

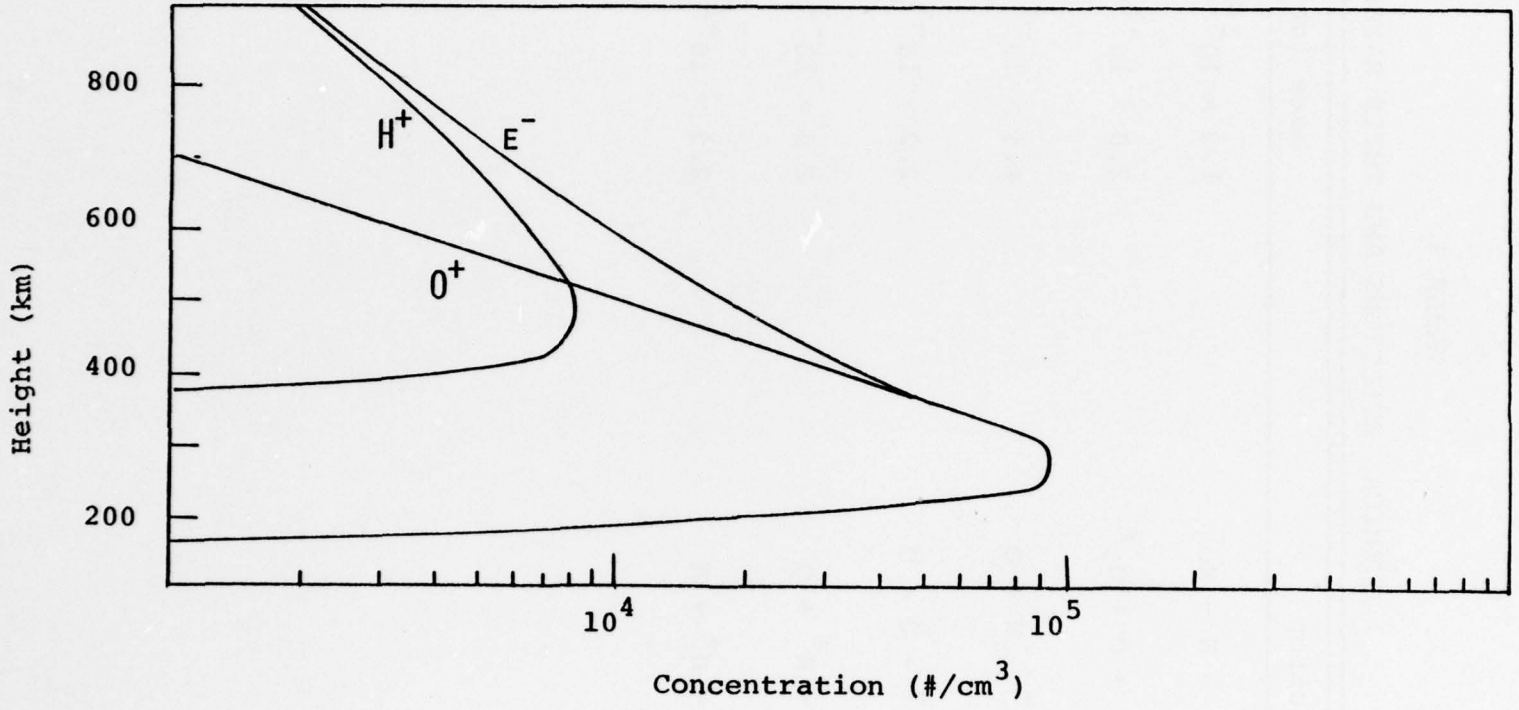

Figure 11. The initial (t = 0) ionospheric density profiles. The electron densities represent measured values at 75.5° Corrected Geomagnetic Latitude on the northern day side in midwinter during quiet magnetic intervals.

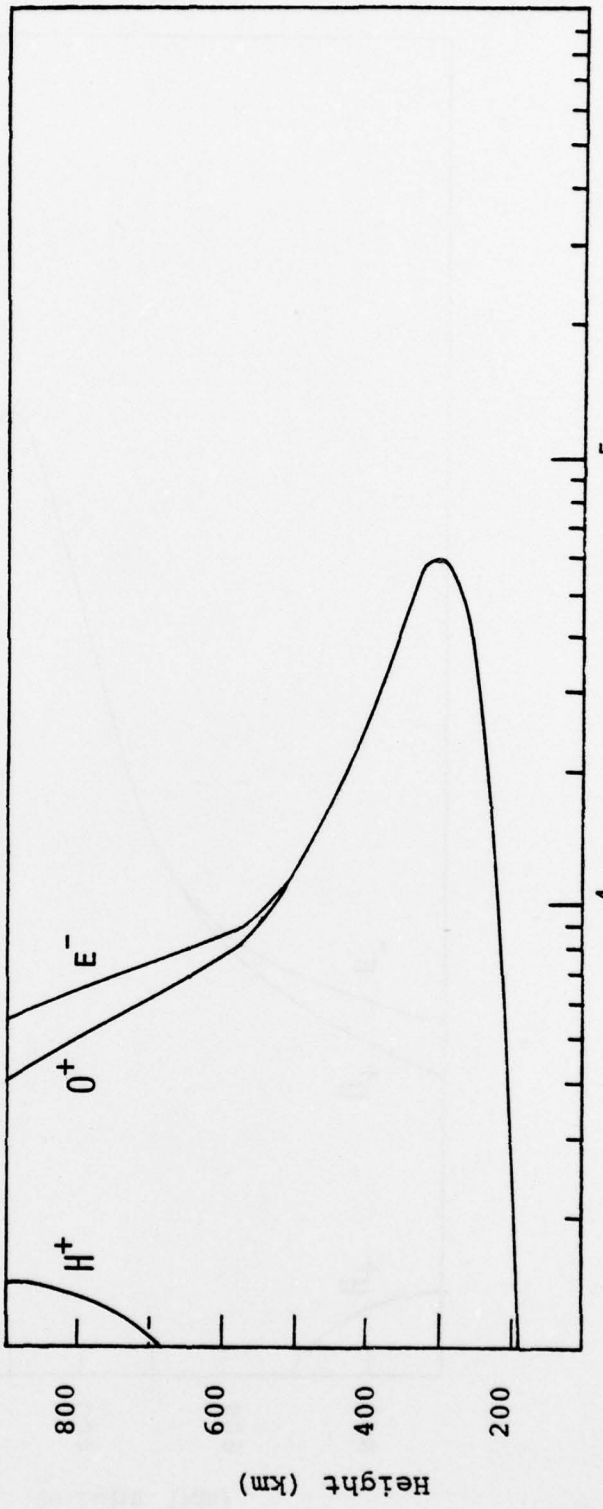

Figure 12. The ionospheric density profiles of e^-, O^+ and H^+ at t = 15 min.

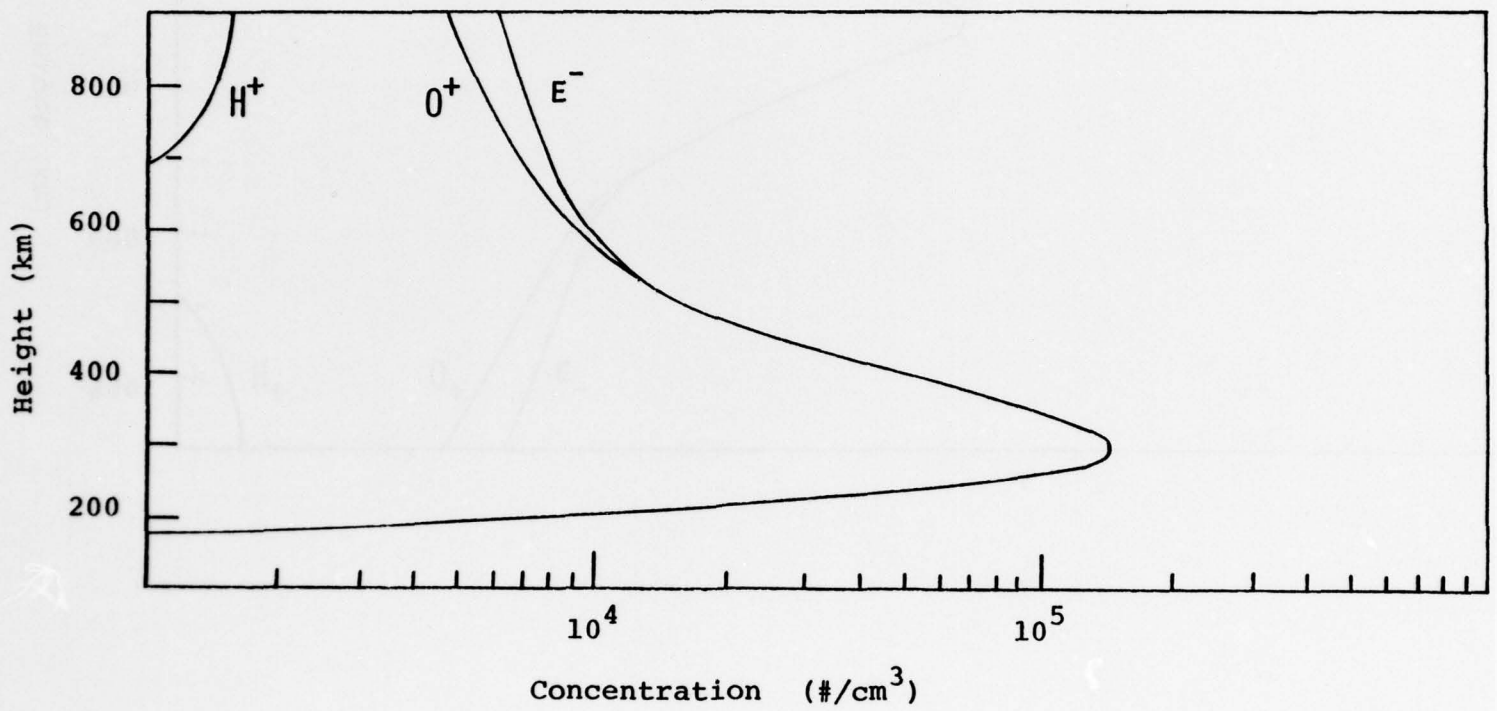

Figure 13. The ionospheric density profiles of e^-, O^+ and H^+ at t = 20 min with O^+ production operating for the last 5 min.

REFERENCES

Akasofu, S.-I., Physics of Magnetospheric Substorms, Reidel Publishing Co., Dordrecht, Holland (1977).

Balko, B. and Michael Mendillo, Finite Element Simulation applied to the transport of Neutral and ionized particles in the Earth's upper atmosphere, Astron. Contrib. Boston Univ. Ser III, No. 1 (1977).

Banks, P.M. and G. Kockarts, Aeronomy, Academic Press, New York, N.Y. (1973).

Banks, P.M., C.R. Chappell and A.F. Nagy, A new model for the interaction of auroral electrons with the atmosphere: spectral degradation, backscatter, optical emission and ionization, J. Geophys. Res., 79, 1459 (1974).

Chacko, C.C. and Michael Mendillo, Electron density enhancements in the F-region beneath the magnetospheric cusp, J. Geophys. Res., 82, 4757 (1977).

Knudsen, W.C., P.M. Banks, J.D. Winningham and D.M. Klumpar, Numerical model of the convecting F_2 ionosphere at high latitudes, J. Geophys. Res., 82, 4784 (1977).

tas G.P. and J.C.Y. Walker, The penetration of soft electrons into the ionosphere, Planet. Space Sci., 24, 409 (1976).

M.H., Auroral ionization and excitation by incident nergetic electrons, Planet. Space Sci., 11, 1209 (1963).